Diffractive Phenomena at HERA [1]

Paul Newman[2] (E-mail address: prn@hep.ph.bham.ac.uk)
for the H1 and ZEUS Collaborations.
School of Physics, University of Birmingham, B15 2TT, UK

Highlights selected from recent measurements of colour-singlet exchange processes at HERA are summarised. Particular emphasis is placed on energy and momentum transfer dependences and the decomposition of the data into an expansion in Regge trajectories. The latest results in vector meson helicity analysis, partonic descriptions of hard diffraction and diffractive dijet production are also covered.

1 Introduction

When discussing the success of the standard model, it is often overlooked that the bulk of hadronic cross sections remain rather poorly understood within the gauge theory of the strong interaction, quantum chromodynamics (QCD). Before the advent of QCD, many aspects of hadronic interactions were understood in the framework of Regge phenomenology, which is based on the most general properties of the scattering matrix. In Regge models, diffractive (elastic, dissociative and, via the optical theorem, total) cross sections are well described [1] at high energy by the exchange of the leading vacuum singularity or *pomeron*. The relationship between Regge asymptotics and QCD is far from clear.

The lepton beam at HERA can be considered as a prolific source of high energy real and virtual photons, such that diffractive scattering in the $\gamma^{(*)}p$ system can be studied. A variety of hard scales can be introduced to the problem, such that HERA provides an excellent opportunity to study diffraction in regions in which perturbative QCD may be applicable. This leads to the exciting possibility of gaining an understanding of diffraction and the pomeron at the level of parton dynamics and of studying the transition between perturbatively calculable and perturbatively incalculable strong interactions. The H1 and ZEUS experiments have produced many new and innovative measurements that have already led to improvements in the QCD description of diffraction. This contribution summarises the most recent developments in colour-singlet exchange physics at HERA. A summary of older results can be found, for example, in [2].

The generic colour-singlet exchange process $\gamma^{(*)}p \to XY$ at HERA is illustrated in figure 1a. The hadronic final state consists of two distinct systems X and Y, with Y being the closer to the outgoing proton direction. The processes principally considered here are exclusive vector meson production $\gamma^{(*)}p \to Vp$ where $V = \rho, \omega, \phi \ldots$ (fig 1b) and semi-inclusive virtual photon dissociation $\gamma^{(*)}p \to Xp$, for all systems X (fig 1c). The semi-inclusive charge exchange reaction $\gamma^*p \to Xn$ is also discussed. Measurements
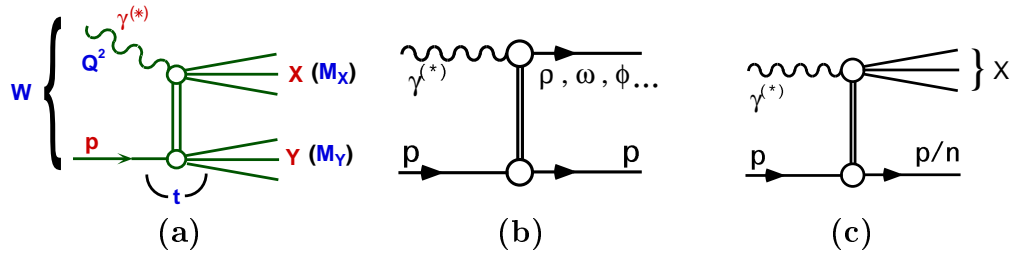

Fig. 1: (a) Illustration of the generic process $\gamma^{(*)}p \to XY$. (b) Exclusive vector meson production $\gamma^{(*)}p \to Vp$. (c) Semi-inclusive colour-singlet exchange $\gamma^{(*)}p \to Xp$ and $\gamma^{(*)}p \to Xn$.

of processes in which the proton dissociates to higher mass systems Y are described elsewhere [3–6].

2   Kinematic Variables

With q and P denoting the 4-vectors of the incoming photon and proton respectively, the standard kinematic variables

$$Q^2 \equiv -q^2 \qquad\qquad x \equiv \frac{Q^2}{2q.p} \qquad\qquad W^2 \equiv (q + P)^2 \ , \qquad (1)$$

are defined. In the context of figure 1a, with p_X and p_Y representing the 4-vectors of the final state systems X and Y respectively, three further variables are introduced;

$$M_X^2 \equiv p_X^2 \qquad\qquad M_Y^2 \equiv p_Y^2 \qquad\qquad t \equiv (P - p_Y)^2 \ , \qquad (2)$$

where t is the squared four-momentum transferred between the photon and the proton. The hermetic nature of the H1 and ZEUS detectors makes it possible to measure all kinematic variables defined in equations 1 and 2 in many circumstances. Where both Q^2 and $|t|$ are small, colour singlet exchange at HERA follows a similar pattern to that in soft hadron-hadron physics [5–8]. The region of large $|t|$ is believed to be a particularly good filter for hard diffractive processes in which the pomeron itself may be perturbatively calculable in terms of the exchange of a pair of gluons from the proton in a net colour-singlet configuration [9]. First measurements in this region are starting to appear [4,10]. This document is principally concerned with the kinematic region in which $|t|$ is small and a large value of Q^2 sets a hard scale.

For virtual photon dissociation $\gamma^*p \to Xp$, the kinematics are usually expressed in terms of the variables

$$x_{\mathbb{P}} \equiv \frac{q \cdot (P - p_Y)}{q \cdot P} = \frac{M_X^2 + Q^2 - t}{W^2 + Q^2 - m_p^2} \qquad\qquad \beta \equiv \frac{Q^2}{2q \cdot (P - p_Y)} = \frac{Q^2}{M_X^2 + Q^2 - t} \ , \quad (3)$$

where m_p is the proton mass. Here, $x_{\mathbb{P}}$ can be interpreted as the fraction of the proton beam momentum transferred to the system X and β may be considered as the fraction

of the exchanged longitudinal momentum that is carried by the quark coupling to the photon.

Where leading baryons are directly tagged (see section 3), the measured quantities are the transverse momentum p_T and energy E'_p of the final state proton or neutron. The kinematic variables used to describe the process are

$$z \equiv 1 - \frac{q.(p - p')}{q.p} \simeq \frac{E'_p}{E_p} \qquad\qquad t \equiv (p - p')^2 \simeq -\frac{p_T^2}{z} - (1 - z)\left[\frac{m_N^2}{z} - m_p^2\right] \ , \quad (4)$$

where p' is the 4-vector of the final state nucleon and m_N is its mass. Provided the final state nucleon is exclusively produced at the proton vertex, the definitions (2) and (4) of t are equivalent and $z = 1 - x_{\mathbb{P}}$.

3   Experimental Techniques

Much of the data presented here is selected on the basis of a large rapidity gap adjacent to the outgoing proton beam, identified by an absence of activity in the more forward [3] parts of the detectors. The resulting data samples are dominated by the case where Y is a proton. This approach yields high acceptance over a wide kinematic region. Since the size of the rapidity gap separating the systems X and Y decreases as M_X grows, measurements by this method are restricted to the region $x_{\mathbb{P}} \lesssim 0.05$ in which diffraction is expected to be dominant.

In a second experimental method, final state baryons are detected directly. Purpose-built forward proton spectrometers (FPSs) are exploited to detect and measure final state protons [11,12]. Calorimetry is also installed along the forward beam-line to detect and measure leading neutrons [12,13]. The direct tagging method allows the system Y to be positively identified as a proton or neutron and is the only way of measuring the t distribution for the photon dissociation process. It also allows access to an enhanced region of $x_{\mathbb{P}}$. However, the incomplete acceptances of the forward proton and neutron detectors limit the available statistics.

The exclusive production of vector mesons is identified through the absence of any activity in the central and backward parts of the detectors beyond that associated with the vector meson decay. The charged decay products of the vector mesons are detected with high resolution in central tracking devices. For the measurements described here, the decay channels $\rho^0 \rightarrow \pi^+\pi^-$, $\phi \rightarrow K^+K^-$, $J/\psi \rightarrow \mu^+\mu^-$ and $J/\psi \rightarrow e^+e^-$ are studied. Measurements have also been made using the decays $\omega \rightarrow \pi^+\pi^-\pi^0$ [14], $\rho' \rightarrow \pi^+\pi^-\pi^+\pi^-$ [15] and various decay modes of $\psi(2S)$ [16]. Observations of the Υ have also recently been reported [17].

In the study of photon dissociation by the rapidity gap or leading baryon tagging methods, the system X is measured in the central parts of the detectors after requiring that there be no calorimetric activity forward of a given pseudorapidity. A third selection procedure is favoured by ZEUS for studies of photon dissociation [8]. Without

---

[3]In the HERA coordinate system, the 'forward' positive z direction is that of the outgoing proton beam and corresponds to positive values of rapidity.

explicitly requiring a forward rapidity gap, the diffractive signal is extracted from the low mass tail in the distribution in hadronic invariant mass M_X visible in the central components of the detector (see section 4.3).

4   Dependences on W and t

4.1   Parameterising Colour Singlet Exchange Cross Sections

The language of Regge phenomenology is generally used to discuss the kinematic dependences of colour singlet exchange cross sections at HERA. This does not necessarily imply the exchange of universal Regge poles. It does, however, provide a convenient means of parameterising the data and comparing processes involving the scattering of different particles at different values of t or Q^2.

Usually, only the minimal asymptotic Regge assumption is needed,[4] which states that with t, M_X and Q^2 fixed,

$$\frac{\mathrm{d}\sigma}{\mathrm{d}t\mathrm{d}M_X^2} \propto \left(\frac{1}{x_{\mathbb{P}}}\right)^{2\alpha_{\mathbb{P}}(t)-2} \quad , \tag{5}$$

where $\alpha_{\mathbb{P}}(t)$ is the *effective leading Regge trajectory* describing the process. Varying $x_{\mathbb{P}}$ at fixed M_X, Q^2 and t is equivalent to varying W^2 (equation 3). Since $W^2 \gg Q^2$ throughout most of the HERA kinematic domain, $1/x_{\mathbb{P}}$ in equation 5 is often replaced simply by W^2.

In order to additionally model the t dependence, it is necessary to introduce the form factors of the interacting particles. These are usually approximated to empirically motivated exponential functions, such that at fixed M_X and Q^2, the full W and t dependence is given by

$$\frac{\mathrm{d}\sigma}{\mathrm{d}t\mathrm{d}M_X^2} \propto \left(\frac{1}{x_{\mathbb{P}}}\right)^{2\alpha_{\mathbb{P}}(t)-2} e^{b_0 t} \sim \left(W^2\right)^{2\alpha_{\mathbb{P}}(t)-2} e^{b_0 t} \quad . \tag{6}$$

For soft diffractive processes, the leading trajectory takes the universal linear form $\alpha_{\mathbb{P}}(t) \sim \alpha(0) + \alpha' t \sim 1.08 + 0.25\ t$ [18]. Where hard scales are present, the effective pomeron intercept $\alpha_{\mathbb{P}}(0)$ is expected to increase and the trajectory slope α' is expected to decrease [19].

4.2   Vector Meson Energy and Momentum Transfer Dependences

Figure 2a shows the centre of mass energy dependence of various t-integrated vector meson cross sections at $Q^2 = 0$ [5, 7, 14, 17, 20–23], after correcting for the small proton dissociation contributions. In common with the total cross section at $Q^2 = 0$ [24], the energy dependence of the ρ^0 photoproduction cross section follows that expected for the exchange of the universal soft pomeron of hadronic physics. In contrast to this, for
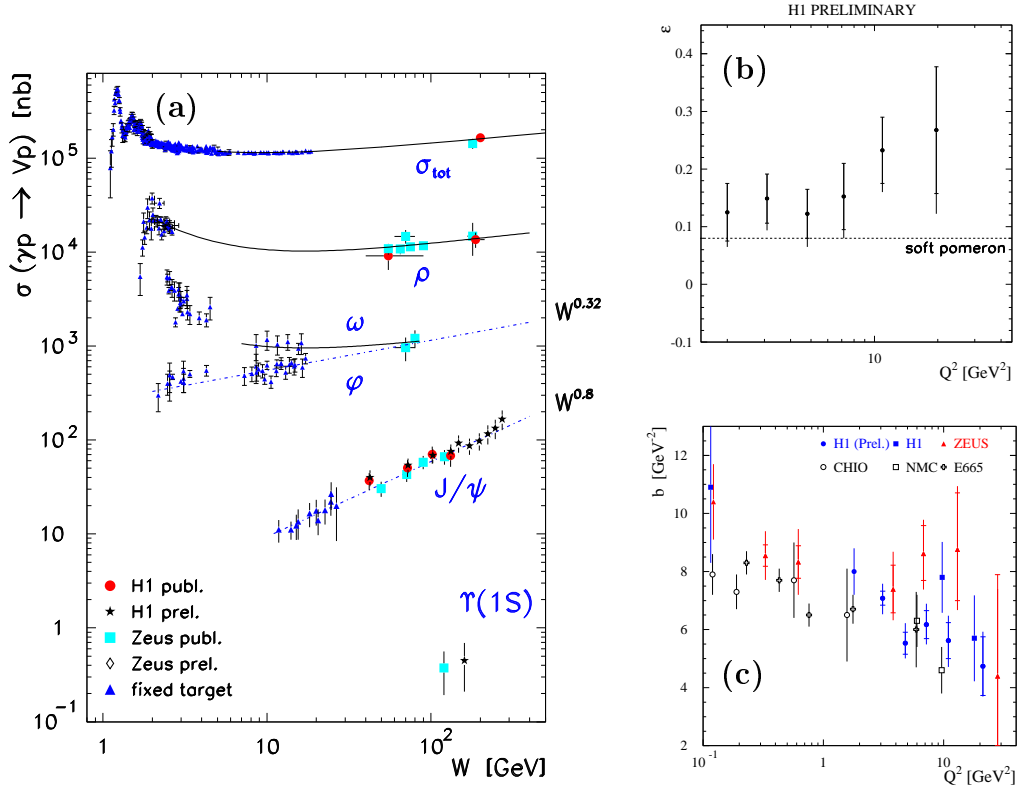
Fig. 2: (a) Various vector meson cross sections shown as a function of W at $Q^2 = 0$, together with the total photoproduction cross section. (b) The Q^2 dependence of the parameter $\epsilon = \alpha_{I\!P}(0) - 1$, extracted from fits to the W dependence of exclusive ρ^0 electroproduction. (c) The Q^2 dependence of the slope parameter b for exclusive ρ^0 electroproduction.

J/ψ photoproduction, where a hard scale corresponding to the charm quark mass is introduced, the W dependence of the cross section is much steeper.

Figure 2b shows the effective pomeron intercept as a function of Q^2 for the process $\gamma^* p \rightarrow \rho^0 p$, as extracted from fits to equation 6 after integration over t. There is evidence for a steepening of the W depedendence of the rho electroproduction cross section as Q^2 increases. It is thus apparent that the introduction of hard scales such as Q^2 or a heavy quark mass leads to an increase in the effective $\alpha_{I\!P}(0)$ describing the vector meson production energy dependence.

The t dependence of vector meson production is studied by fitting data to the form $\mathrm{d}\sigma/\mathrm{d}t \propto e^{bt}$, where in the context of equation 6, $b = b_0 + 2\alpha' \ln(W^2/\mathrm{GeV}^2)$. The extracted value of b for ρ production is shown as a function of Q^2 in figure 2c. There

---

[4]Triple Regge analysis has been applied to diffractive dissociation in photoproduction [6,8].

is a clear decrease of b with increased Q^2. This indicates that the $\gamma^* \to V$ transition becomes an increasingly short distance process as Q^2 is increased. For the case of J/ψ photoproduction, $b \sim 4.5$ GeV^{-2}, similar to that for the ρ at large Q^2, again indicating that exclusive J/ψ electroproduction is already a hard process at $Q^2 = 0$.

4.3   The Diffractive Dissociation Cross Section at Low $x_{\mathrm{I\!P}}$

The t dependence of the virtual photon dissociation process has been measured in the diffraction dominated low $x_{\mathrm{I\!P}}$ region using the ZEUS FPS [25]. The data are shown in figure 3a, together with a fit to the form $\mathrm{d}\sigma/\mathrm{d}t \propto e^{bt}$. The result is $b = 7.2 \pm 1.1$ (stat.) $^{+0.7}_{-0.9}$ (syst.) GeV^{-2}, revealing a highly peripheral scattering characteristic of a diffractive process.
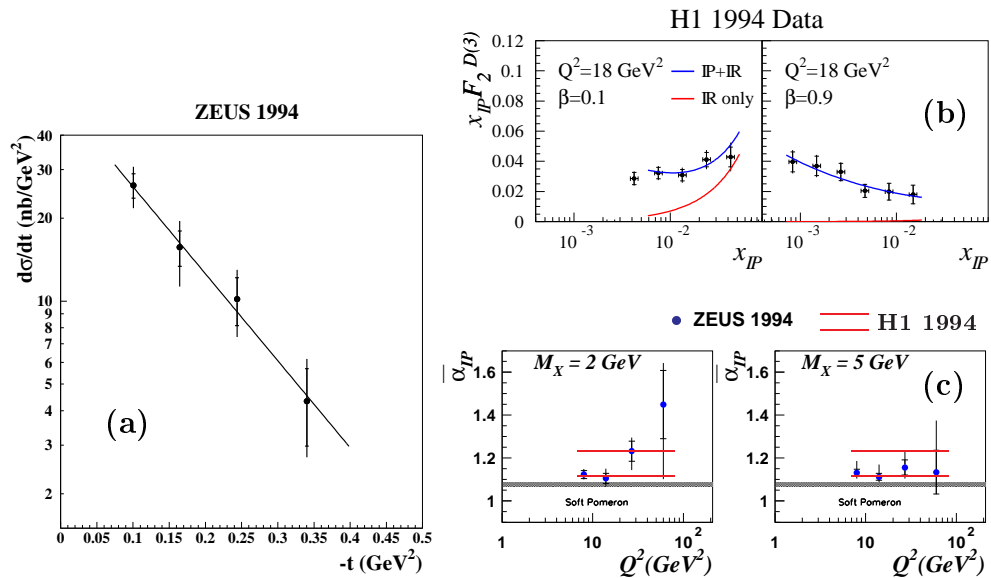

Fig. 3: (a) Differential t-distribution in the kinematic region $5 < Q^2 < 20$ GeV^2, $0.015 < \beta < 0.5$ and $x_{\mathrm{I\!P}} < 0.03$, obtained using the ZEUS FPS. (b) Example H1 measurements of $x_{\mathrm{I\!P}} \cdot F_2^{D(3)}$, together with the results of a fit to the parameterisation of equations 9 and 10. (c) Comparison of H1 and ZEUS extractions of $\alpha_{\mathrm{I\!P}}(0)$ for virtual photon dissociation, together with the value expected for the 'soft' pomeron that governs hadronic interactions in the absence of hard scales.

Virtual photon dissociation data obtained by the rapidity gap technique are usually presented in the form of a three dimensional structure function $F_2^{D(3)}(\beta, Q^2, x_{\mathrm{I\!P}})$, defined in close analogy to the inclusive proton structure function as

$$F_2^{D(3)}(\beta, Q^2, x_{\mathrm{I\!P}}) = \frac{\beta Q^4}{4\pi\alpha^2} \; \frac{1}{(1 - y + y^2/2)} \; \int_{t_0}^{t_{\min}} \mathrm{d}t \; \frac{\mathrm{d}^4\sigma^{ep \to eXY}}{\mathrm{d}\beta \; \mathrm{d}Q^2 \; \mathrm{d}x_{\mathrm{I\!P}}\mathrm{d}t} \; . \qquad (7)$$

Measurements of $F_2^{D(3)}$ have been made by H1 using the rapidity gap technique at 356 points in β, Q^2 and $x_{\mathbb{P}}$ space, spanning the region $0.001 < \beta < 0.9$ and $0.4 < Q^2 < 800 \text{ GeV}^2$, integrated over $M_Y < 1.6 \text{ GeV}$ with $t_0 = -1.0 \text{ GeV}^2$ [26, 27]. For a single universal exchange, a factorisation of the $x_{\mathbb{P}}$ dependence is expected of the form [28]

$$F_2^{D(3)} = f_{\mathbb{P}/\mathrm{p}}(x_{\mathbb{P}}) \ F_2^{\mathbb{P}}(\beta, Q^2) \ , \tag{8}$$

where, for a cross section differential in $x_{\mathbb{P}}$, after integrating equation 6 over t,

$$f_{\mathbb{P}/\mathrm{p}}(x_{\mathbb{P}}) \propto \int_{-1\,\mathrm{GeV}^2}^{t_0(x_{\mathbb{P}})} \left(\frac{1}{x_{\mathbb{P}}}\right)^{2\alpha_{\mathbb{P}}(t)-1} e^{B_{\mathbb{P}} t} \ \mathrm{d}t \tag{9}$$

parameterises the flux factor for the exchange i from the proton. Here, $B_{\mathbb{P}} = b_0 + 2\alpha' \ln(1/x_{\mathbb{P}})$ in equation 6. In equation 8, $F_2^{\mathbb{P}}(\beta, Q^2)$ may be interpreted as being proportional to the structure function of the pomeron [28].

When viewed in close detail, the data do no quite obey the factorisation of equation 8. As an example, data at $Q^2 = 18 \text{ GeV}^2$ and two different values of β are shown in figure 3b. At fixed Q^2, a variation in the $x_{\mathbb{P}}$ dependence of $F_2^{D(3)}$ is observed as β changes. In a Regge model, this is interpreted in terms of the exchange of sub-leading trajectories in addition to the pomeron when $x_{\mathbb{P}}$ becomes large. Table 1 summarises the trajectories that have most commonly been considered in soft hadronic physics. In a more complete Regge treatment, the differential structure function then follows [5]

$$F_2^{D(3)} = \sum_{i=\mathbb{P},\mathbb{R},\pi\ldots} f_{i/\mathrm{p}}(x_{\mathbb{P}}) \ F_2^i(\beta, Q^2) \tag{10}$$

where $f_{i/\mathrm{p}}$ is a flux factor for the exchange i, similar in form to equation 9.

TRAJECTORY	APPROX. $\alpha(0)$	APPROX α'	ISOSPIN	$p : n$
$\mathbb{P}$	1	0.25	0	1 : 0
f, ω	0.5	1.0	0	1 : 0
ρ, a	0.5	1.0	1	1 : 2
π	0	1.0	1	1 : 2

Table 1 Summary of commonly discussed Regge trajectories, together with their approximate intercepts and slopes, their isospin and the expected ratio of fluxes for leading proton and neutron production. The exchange degenerate f, ω, ρ and a trajectories are collectively referred to as $\mathbb{R}$.

Allowing for the exchange of one further trajectory ($\mathbb{R}$) in addition to the pomeron is sufficient to obtain a good description of $F_2^{D(3)}$ throughout the measured kinematic range. In fits to intermediate Q^2 data [26] based on equation 10 in which $\alpha_{\mathbb{P}}(0)$, $\alpha_{\mathbb{R}}(0)$ and the values of $F_2^{\mathbb{P}}$ and $F_2^{\mathbb{R}}$ at each (β, Q^2) point are free parameters, the

---

[5]Interference terms are also possible, in particular, that between $\mathbb{P}$ and f. In [26], there was found to be little sensitivity to the presence or absence of this term.

intercept of the secondary trajectory is found to be $\alpha_{\mathrm{IR}}(0) = 0.50 \pm 0.11$ (stat.) $\pm$ 0.11 (syst.)$^{+0.09}_{-0.10}$ (model), consistent with the exchange of the f or one of its exchange degenerate partners.

In their analysis of virtual photon dissociation, ZEUS fit the hadronic invariant mass distribution at fixed W and Q^2, to the form

$$\mathrm{d}\mathcal{N}/\mathrm{d}\ln M_X^2 = D + c\, e^{b\ln M_X^2} \ , \qquad (11)$$

where the second term parameterises the contribution from non-diffractive processes at large M_X. The operationally defined diffractive contribution D is acceptance corrected to give the cross section in intervals of M_X, W^2 and Q^2 for the process $ep \to eXY$ with $M_Y < 5.5$ GeV [8]. The W dependence of the diffractive contribution at fixed Q^2 and M_X [6] is then used to extract the t averaged value of the pomeron intercept, $\overline{\alpha_{\mathrm{IP}}}$, by fitting to the form

$$\frac{\mathrm{d}\sigma^{ep\to eXY}}{\mathrm{d}M_X}(M_X,W,Q^2) \propto \left(W^2\right)^{2\,\overline{\alpha_{\mathrm{IP}}}-2} \ , \qquad (12)$$

derived from equation 5. The results are shown in figure 3c and are compared with the H1 result, $\alpha_{\mathrm{IP}}(0) = 1.203 \pm 0.020$ (stat.) ± 0.013 (syst.) $^{+0.030}_{-0.035}$(model), amended to $\overline{\alpha_{\mathrm{IP}}}$ assuming $b = 7.2 \pm 1.4$ GeV^{-2} [25] and $\alpha'_{\mathrm{IP}} = 0.26 \pm 0.26$ GeV^{-2}. The two experiments are found to be in good agreement. The effective pomeron intercept is significantly larger than the values $\alpha_{\mathrm{IP}} \sim 1.1$ obtained from soft diffractive processes [18] and is similar to that describing exclusive J/ψ photoproduction. To date, there is no evidence for a variation of the effective $\alpha_{\mathrm{IP}}(0)$ with Q^2 within the deep-inelastic regime. However, the values extracted from photon dissociation at $Q^2 = 0$ are significantly smaller [6,8].

4.4   Leading baryons at Large x_{IP}

The extensive coverage in final state baryon energy of the leading proton and neutron detectors allows the study of colour singlet exchange processes to be extended to the region of comparatively large x_{IP} (equivalently small z - see equation 4), which in Regge models is expected to be dominated by sub-leading exchanges.

A large fraction of DIS events are found to contain forward baryons in the final state outside the large z diffractive region. For example, ZEUS find [31] that approximately 12.5 % of events have a leading proton or neutron with $0.6 < z < 0.9$ scattered through a polar angle $\theta < 0.8$ mrad. Fragmentation models [29,30] that are successful in describing energy flow in the photon fragmentation and central plateau regions fail to reproduce the rates and energy distributions of the low z leading baryons.

H1 define leading proton and neutron structure functions, $F_2^{LP(3)}$ and $F_2^{LN(3)}$ respectively, in a similar way to $F_2^{D(3)}$;

$$F_2^{LB(3)}(x,Q^2,z) = \frac{xQ^4}{4\pi\alpha^2}\,\frac{1}{1-y+y^2/2}\int_{t_{200}}^{t_{\min}}\frac{\mathrm{d}^4\sigma^{ep\to eXN}}{\mathrm{d}x\,\mathrm{d}Q^2\,\mathrm{d}z\mathrm{d}t} \ , \qquad (13)$$

---

[6]The variable β is thus also fixed.

where the integration limit t_{200} is defined through equation 4 by the condition $p_T = 200$ MeV. The differential structure function is measured in the region $0.6 < z < 0.9$ in 12 bins of x and Q^2, one of which is shown in figure 4a [12]. ZEUS perform a similar analysis for data integrated over x in two regions of Q^2. They have also measured the t dependence of leading baryon production at low z [31]. Figure 4b shows the z dependence of the slope parameter b, obtained by fitting the leading proton data to the standard exponential form $\mathrm{d}\sigma/\mathrm{d}t \propto e^{bt}$.
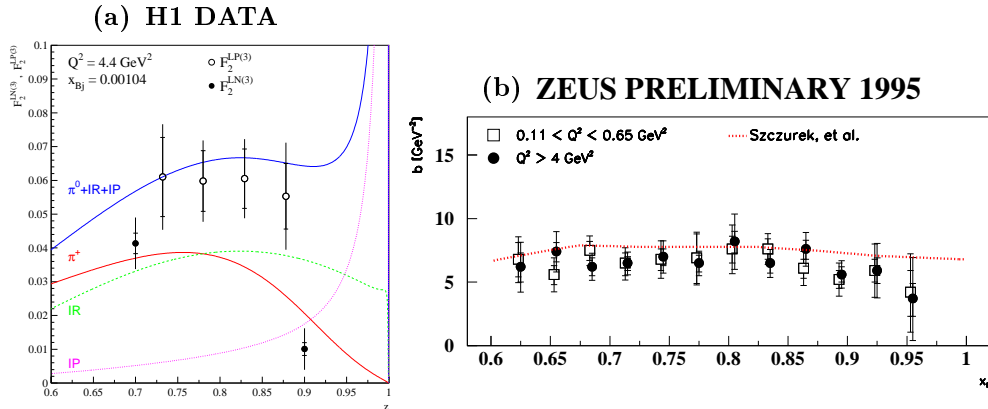

Fig. 4: (a) Dependence of the leading proton (open points) and neutron (closed points) structure functions on z in an example bin of x and Q^2. The decomposition of the data according to a Regge model is superimposed. (b) Dependence of the t slope parameter on z, with a comparison to a similar model.

Both collaborations compare their low z leading baryon measurements with simple Regge pole models. The trajectories considered are summarised in table 1. The exchange of isoscalar trajectories leads to the production of leading protons only. Isovector exchanges yield protons and neutrons in the ratio $1:2$. Contributions from proton dissociative processes are neglected, but have been shown to be small [12].

The rate of leading proton production is larger than that for leading neutron production throughout the region $0.6 < z < 0.9$ (figure 4a). This implies that leading protons in this region are dominantly produced by an isospin-0 exchange. The contributions from ρ and a exchanges must therefore be small and the models accordingly consider only $\mathbb{P}$, $\mathbb{R} \equiv f$, ω and π exchange. With this combination of exchange trajectories, the data are compared to models similar in form to equation 10, with assumptions regarding flux factors and structure functions as specified in [32]. The breakdown of the cross section into different exchange contributions is shown in figure 4a. The predicted z dependence of the t slope parameter is superimposed in figure 4b. Given that there are no free parameters in these models, the agreement with data is remarkably good. For leading proton production, the $\mathbb{R}$ contribution is found to be approximately twice as large as the π contribution, with the $\mathbb{P}$ exchange contribution smaller still for $z \lesssim 0.9$. The neutron production cross section is saturated by the prediction for π exchange.

5 Vector Meson Helicity Analyses

Full extractions of the 15 spin density matrix elements governing vector meson electro-production [33] have recently been made. The spin density matrix elements describe the transitions between the helicity components of the initial state photon and proton and the final state vector meson and proton.
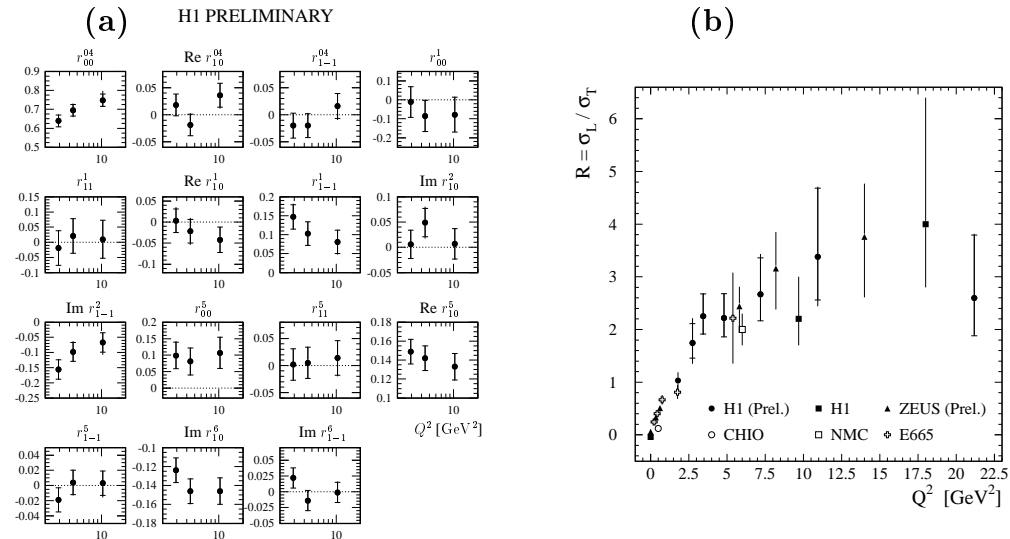

Fig. 5: (a) The full set of spin density matrix elements, shown for ρ electroproduction as a function of Q^2. The dashed lines show the expected values assuming SCHC and NPE. (b) The ratio of longitudinal to transverse photon induced cross sections $\gamma^* p \to \rho p$, derived from equation 14, shown as a function of Q^2.

Figure 5 shows the spin density matrix elements for the ρ at three different values of Q^2 as extracted by H1 [34]. The hypothesis of s-channel helicity conservation (SCHC) states that the produced vector meson should retain the polarisation of the incoming photon. The hypothesis of natural parity exchange (NPE) states that the quantum numbers exchanged in the t channel should have positive parity. Both hypotheses are usually expected to hold for diffractive processes [35]. Where appropriate in figure 5, the dashed lines show the expected values of the spin density matrix elements for the case of SCHC and NPE. There is a significant deviation from the expected value of zero for the matrix element r_{00}^5. This deviation is also observed by ZEUS for both ρ and ϕ production [36]. It implies that there is a non-zero probability for longitudinally polarised photons to yield transversely polarised ρ mesons. H1 measure the ratio of single helicity flip to helicity conserving amplitudes to be $8 \pm 3\%$. The magnitude of the helicity flip amplitude has been predicted in a QCD inspired model [37], giving further confidence that perturbative approaches become applicable to vector meson production where hard scales are introduced.

Assuming SCHC, the matrix element r_{00}^{04} is related to the ratio of cross sections R for longitudinal to transverse photons according to

$$R = \frac{\sigma_{\mathrm{L}}}{\sigma_{\mathrm{T}}} = \frac{1}{\epsilon} \frac{r_{00}^{04}}{1 - r_{00}^{04}} \ , \tag{14}$$

where the polarisation parameter $\epsilon \sim 0.99$ at HERA. The breaking of s-channel helicity conservation has only a small effect on the value of R extracted by this method. Figure 5b shows a compilation of HERA and fixed target results for R, extracted using equation 14, as a function of Q^2. The increase in R with Q^2 is found to flatten at large Q^2.

6 Partonic Interpretations of Colour Singlet Exchange

6.1 Vector Mesons and the Gluon Structure of the Proton

Diffractive vector meson production follows a similar description to elastic hadron-hadron scattering where no hard scales are present. However, when the scales Q^2, t or the mass of the valence quarks in the vector meson become large, deviations from soft pomeron behaviour become apparent (see sections 4.2 and 5). In such cases, it is natural to attempt to make a perturbative QCD description. The usual approach is to consider the diffractive scattering of the $q\bar{q}$ fluctuation of the photon, which subsequently collapses into the vector meson state. The simplest way to generate a colour singlet exchange at the parton level is via the exchange of a pair of gluons. Several authors have built models of hard vector meson production that contain the square of the gluon distribution of the proton [19, 37]. These models are able to give good descriptions of the data [23, 38]. Particularly for the ρ, the success of two-gluon exchange models is tempered by theoretical uncertainties such as that associated with the vector meson wavefunction.

6.2 Two Gluon Exchange Models and Virtual Photon Diffractive Dissociation

The success of two-gluon exchange models in describing hard vector meson production motivates a similar approach to virtual photon diffractive dissociation. The added complication compared to the vector meson process is that more complex partonic fluctuations of the photon such as $q\bar{q}g$ are expected to play a role [39] in addition to the simplest $q\bar{q}$ state. A recent QCD motivated parameterisation of the diffractive structure function in terms of the diffractive scattering of $q\bar{q}$ and $q\bar{q}g$ states [40] is compared to ZEUS measurements at a fixed small value of $x_{\mathbb{P}}$ in figure 6b. In this model, the medium β region is populated dominantly by $q\bar{q}$ final states originating from transversely polarised photons. The $q\bar{q}g$ photon fluctuations are most significant at low β. Finally, there is a significant higher twist contribution at large β and low Q^2, generated by the interaction of longitudinally polarised photons.
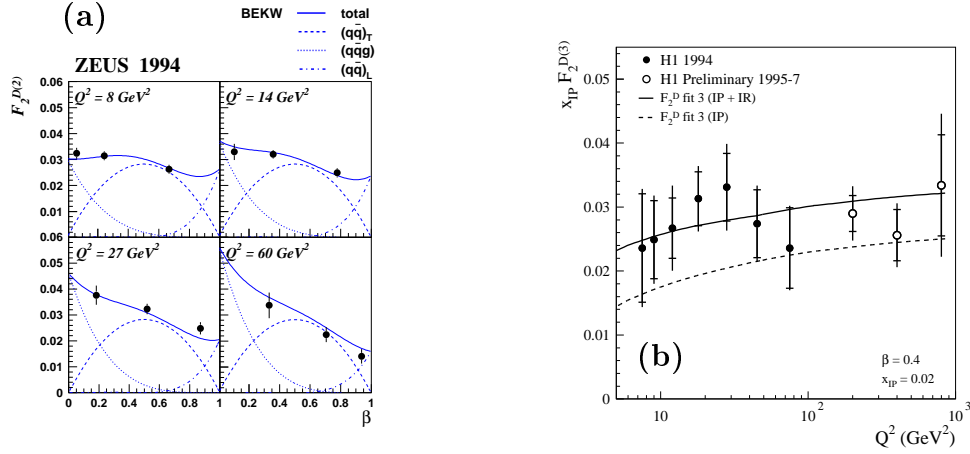
Fig. 6: (a) ZEUS measurement of the β dependence of $F_2^{D(3)}$ at various values of Q^2 and $x_{\mathbb{P}} = 0.0042$, compared to a model based on the diffractive scattering of partonic fluctuations of the photon. (b) H1 measurement of the Q^2 dependence of $x_{\mathbb{P}} F_2^{D(3)}$ at $\beta = 0.4$ and $x_{\mathbb{P}} = 0.02$. The results of a DGLAP fit to the 1994 data in which both quarks and gluons contribute at the starting scale for evolution are also shown.

6.3   Diffractive Parton Distributions

In Regge models that consider the exchanged trajectories as distinct partonic systems [28], the β and Q^2 dependences of F_2^D at fixed $x_{\mathbb{P}}$ are sensitive to the parton distributions of the exchanges. The β dependence is relatively flat (figure 6a), with significant contributions at large fractional momenta. An example of the Q^2 dependence at fixed β and $x_{\mathbb{P}}$ is shown in figure 6b. Scaling violations with positive $\partial F_2^D / \partial \log Q^2$ persist to large values of $\beta \gtrsim 0.4$ and extend to large $Q^2 \geq 800$ GeV^2. In factorisable partonic pomeron models, these features indicate the need for a significant 'hard' (large $z_{\mathbb{P}} \equiv x_{g/\mathbb{P}}$) gluon contribution to the pomeron structure.

The H1 fits to the $x_{\mathbb{P}}$ dependence (equation 10) have been extended to describe the β and Q^2 dependence of all data with $4.5 \leq Q^2 \leq 75$ GeV^2 in terms of parton distributions for the pomeron. Singlet quark and gluon distributions are parameterised at a starting scale $Q_0^2 = 3$ GeV^2 and are evolved to larger Q^2 using the DGLAP equations [26]. The results from the best fit of this type are shown in figure 6b. The cross section in the newly measured region $200 \leq Q^2 \leq 800$ GeV^2 [27] is also well described by the extrapolated predictions based on the fits at lower Q^2. Though the precise shape of the parton distributions are rather uncertain at large $z_{\mathbb{P}}$, more than 80 % of the pomeron momentum is carried by gluons throughout the Q^2 range studied in all such acceptable fits.

6.4 The Pion Structure Function

Since the leading neutron cross section can be generated entirely from the π exchange prediction within the Regge model described in section 4.4, the quantity

$$F_2^{LN(3)}(\beta, Q^2, z = 0.7)/\Gamma_\pi(z = 0.7) \tag{15}$$

may be interpreted as a structure function for the pion, where $\Gamma_\pi(z) = \int f_{\pi/p}(z, t)\, \mathrm{d}t$ is the pion flux at $z = 0.7$. Under this assumption, an extraction of F_2^π is shown in figure 7 in a previously unexplored low-x region. The GRV parameterisation [41] matches the data well.
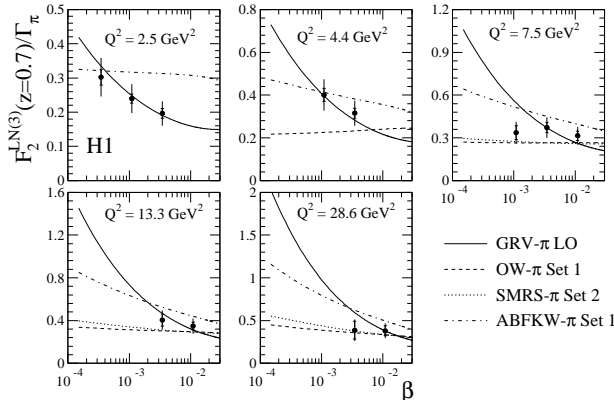

Fig. 7: An extraction of the quantity $F_2^{LN(3)}(\beta, Q^2, z = 0.7)/\Gamma_\pi(z = 0.7)$, which may be interpreted as the structure function of the pion in the Regge model described in section 4.4.

7 Hadronic Final States of Deep-Inelastic Diffraction

Many final state observables are sensitive to the partonic structure of the diffractive interaction and can be used to constrain QCD motivated models. The natural frame in which to study the final state is the rest frame of the system X ($\gamma^\star I\!\!P$ centre of mass frame), the natural direction in that frame being the $\gamma^\star I\!\!P$ collision axis. First HERA results have appeared on event shapes [42], energy flow and charged particle spectra [43], charged particle multiplicities and their correlations [44], dijet production [45, 46] and charm yields [47].

A summary of most of these measurements can be found in [2]. They have confirmed that there are large contributions for which the system X is built from more complex partonic structures than $q\bar{q}$ at lowest order, in particular, at large values of M_X and where large transverse momenta are generated. In the language of a partonic pomeron, all of these measurements confirm that the diffractive parton distributions are dominated by gluons carrying large fractions of the exchanged momentum, boson-gluon fusion (BGF) being the dominant hard process.

7.1 Diffractive Dijet Production

Dijet production is taken here as an example of recent HERA diffractive final state data. The study of dijets is particularly sensitive to the gluon induced BGF process. The jet transverse momenta p_T^{jet} introduce a further hard scale to the problem, testing the universality of the parton distributions extracted from F_2^D and allowing hard diffraction to be tested at $Q^2 = 0$ as well as in DIS. Estimators x_γ^{jets} and $z_{\mathrm{IP}}^{\mathrm{jets}}$ of the photon and pomeron momenta that are transferred to the dijet system can be obtained as described in [45, 46].

Figure 8a shows a measurement of the pseudorapidity distribution of diffractively produced dijets in photoproduction [45]. A combined leading order DGLAP fit is performed to the dijet data at a scale E_t and a measurement [48] of $F_2^{D(3)}$. The relatively high rate of dijet production cannot be reproduced with a quark dominated pomeron. Good fits are obtained with a variety of parameterisations in which a 'hard' gluon distribution dominates the pomeron structure.
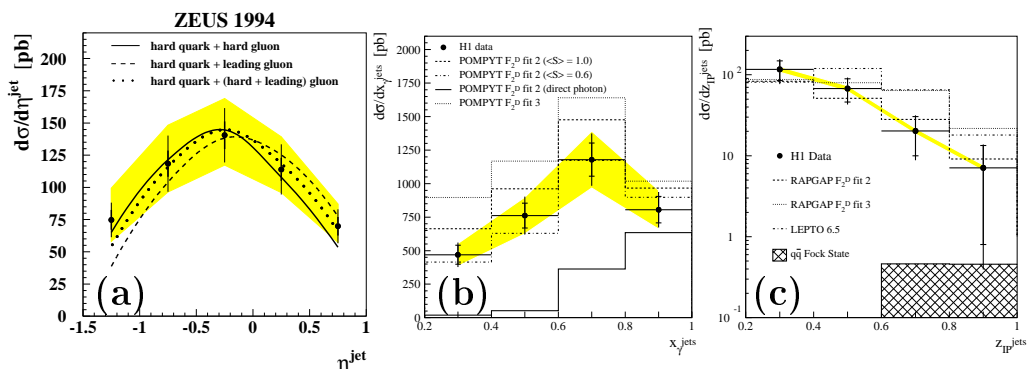

Fig. 8: (a) The diffractive dijet photoproduction cross section differential in pseudorapidity. The results of combined fits to the dijet data and to a measurement of F_2^D, in which the pomeron has a gluon dominated structure, are superimposed. (b) Differential cross section for diffractive dijet photoproduction as a function of x_γ^{jets}. The data are compared with the predictions of the POMPYT Monte Carlo model, based on two sets of gluon dominated pomeron parton distributions. The effect of possible rapidity gap destruction due to spectator interactions in resolved photon interactions is shown by applying a constant weighting factor $\langle S \rangle = 0.6$ to all resolved photon interactions in the simulation. (c) Differential cross section for diffractive dijet electroproduction as a function of $z_{\mathrm{IP}}^{\mathrm{jets}}$. The data are compared to the RAPGAP model based on two gluon dominated sets of parton distributions, to the LEPTO model in which BGF also dominates and to a model [52] of the exclusive production of $q\bar{q}$ final states.

Figure 8b shows the x_γ^{jets} distribution in photoproduction [46]. There are clear contributions from resolved as well as direct photon interactions. Compared through the POMPYT [49] Monte Carlo model with partonic models of the pomeron, it is clear that quark dominated parton distributions underestimate the dijet rates by large factors. The gluon dominated partons derived from the QCD fits to F_2^D (section 6.3)

give a fair description of the data with p_T as the factorisation scale. In the region dominated by resolved photon interactions ($x_\gamma^{\text{jets}} \lesssim 0.8$), there is some evidence for an excess in the prediction, which may be related to rapidity gap destruction effects [50].

Figure 8c shows the $z_{\mathbb{P}}^{\text{jets}}$ distribution in DIS [46]. There are significant contributions in the region of large $z_{\mathbb{P}}^{\text{jets}}$, as expected for the dominance of gluons with large fractional momenta in the exchange. The data are compared through the Monte Carlo program RAPGAP [51] with the gluon dominated pomeron parton distributions extracted from F_2^D. Once again, a good description of the data is obtained with the factorisation scale taken to be p_T. A two-gluon exchange model [52], containing only the $q\bar{q}$ fluctuation of the photon fails to produce the large contributions at low $z_{\mathbb{P}}^{\text{jets}}$, indicating that in this picture, more complex states such as $q\bar{q}g$ are required to generate the large p_T and M_X dijet final states.

8 Summary

The HERA experiments have produced a large volume of data concerned with diffraction and colour-singlet exchange. The kinematic range covered and precision of data on exclusive vector meson production and virtual photon dissociation is continually increasing.

The effective pomeron intercept describing the centre of mass energy dependence at fixed M_X and $t = 0$ becomes larger where hard scales such as Q^2 or a heavy quark mass are introduced. Together with numerous other observations, this motivates a perturbative QCD based approach. For the case of exclusive vector meson production, models based on the fluctuation of the photon into a $q\bar{q}$ pair and the subsequent exchange of a pair of gluons taken from the proton parton distributions successfully reproduce the enhanced energy dependence and other aspects of the problem. For the case of virtual photon dissociation, models of this type can also describe the data, provided the fluctuation of the photon to $q\bar{q}g$ states is also considered.

Where large diffractive final state masses are produced, further exchanges, in addition to the pomeron, are in evidence. It is possible to decompose the data into contributions from a series of Regge exchanges, with pomeron, f and π exchange all being significant in leading proton production. The leading neutron cross section is saturated by the expectations for π exchange.

In models in which partonic substructure is ascribed to the exchanges, evolving according to the DGLAP equations, the pomeron structure is found to be dominated by gluons carrying large fractions of the exchanged momentum. This conclusion is confirmed through the measurement of final state observables such as dijet rates. The leading neutron cross section has been used to extract a structure function for the pion.

Complete analyses of the helicity structure of vector meson production processes have now been made. In the high Q^2 regime, the cross section for ρ and ϕ production by longitudinal photons becomes much larger than that for transverse photons. In this region, clear evidence is found for a violation of the s channel helicity conservation hypothesis.

Acknowledgements

Thanks to Dusan Bruncko and his team for organising such a pleasant conference, to Richard Maraček for showing me the darker sides of Eastern Slovakia and Pavel Murin for putting my life at risk in the High Tatras mountains! I am also grateful to Martin Erdmann and Paul Thompson for proof reading this document.

References

[1] K. Goulianos, *Phys. Rev.* **101** (1983) 169.

[2] P. Newman, *hep-ex/9707020*.

[3] H1 Collab., S. Aid et al., *Nucl. Phys.* **B472** (1996) 3.
     H1 Collab., C. Adloff et al., *Zeit. Phys.* **C75** (1997) 607.

[4] ZEUS Collab., Conf. Paper 788, 29th Intern. Conf. on HEP, Vancouver, Canada (1998).

[5] ZEUS Collab., J. Breitweg et al., *Eur. Phys. J* **C2** (1998) 247.

[6] H1 Collab., C. Adloff et al., *Zeit. Phys.* **C74** (1997) 221.

[7] H1 Collab., S. Aid et al., *Nucl. Phys.* **B463** (1996) 3.

[8] ZEUS Collab., J. Breitweg et al., *Zeit. Phys.* **C75** (1997) 421.

[9] F. Low, *Phys. Rev.* **D12** (1975) 163.
     S. Nussinov, *Phys. Rev. Lett.* **34** (1975) 1286.

[10] ZEUS Collab., M. Derrick et al., *Phys. Lett.* **B369** (1996) 55.
     H1 Collab., paper 274 at Int. Europhys. Conf. on HEP, Jerusalem, August 1997.
     H1 Collab., paper 380 at Int. Europhys. Conf. on HEP, Jerusalem, August 1997.
     H1 Collab., Conf. Paper 570, 29th Intern. Conf. on HEP, Vancouver, Canada (1998).

[11] ZEUS Collab., M. Derrick et al., *Z. Phys* **C73** (1997) 253.

[12] H1 Collab., C. Adloff et al., DESY **98-169**, submitted to *Eur. Phys. J. C.*

[13] S. Bhadra et al., *Nucl. Instr. and Meth* **A394** (1997) 121.

[14] ZEUS Collab., M. Derrick et al., *Zeit. Phys.* **C73** (1996) 73.

[15] H1 Collab., Conf. Paper pa01-088, 28th Intern. Conf. on HEP, Warsaw, Poland (1996).

[16] H1 Collab., C. Adloff et al., *Phys. Lett.* **B421** (1998) 385.
     H1 Collab., Conf. Paper 572, 29th Intern. Conf. on HEP, Vancouver, Canada (1998).

[17] ZEUS Collab., J. Breitweg et al., *Phys. Lett.* **B437** (1998) 432.
     H1 Collab., Conf. Paper 574, 29th Intern. Conf. on HEP, Vancouver, Canada (1998).

[18] A. Donnachie, P. Landshoff, *Phys. Lett.* **B296** (1992) 227.

[19] L. Frankfurt et al., *Phys. Rev.* **D54** (1996) 3194.
     A. Martin et al., *Phys. Rev.* **D55** (1997) 4329.
     I. Royen, J. Cudell, *hep-ph/9807294*.

[20] ZEUS Collab., M. Derrick et al., *Phys. Lett.* **B377** (1996) 259.

[21] H1 Collab., S. Aid et al., *Nucl. Phys.* **B472** (1996) 3.

[22] ZEUS Collab., J. Breitweg et al., *Z. Phys.* **C75** (1997) 215.

[23] H1 Collab., Conf. Paper 572, 29th Intern. Conf. on HEP, Vancouver, Canada (1998).

[24] ZEUS Collab., M. Derrick et al., *Z. Phys.* **C63** (1994) 391.
     H1 Collab., S. Aid et al., *Z. Phys.* **C69** (1995) 27.

[25] ZEUS Collab., J. Breitweg et al., *Eur. Phys. J.* C1 (1998) 81.

[26] H1 Collab., C. Adloff et al., *Zeit. Phys.***C76** (1997) 613.

[27] H1 Collab., Conf. Paper 571, 29th Intern. Conf. on HEP, Vancouver, Canada (1998).

[28] G. Ingelman, P. E. Schlein, *Phys. Lett.* **B152** (1985) 256.

[29] L. Lönnblad, *Comput. Phys. Commun.* **71** (1992) 15.

[30] G. Ingelman et al., *Comput. Phys. Commun.* **101** (1997) 108.

[31] ZEUS Collab., Conf. Paper 789, 29th Intern. Conf. on HEP, Vancouver, Canada (1998).

[32] A. Szczurek et al., *Phys. Lett.* **B428** (1998) 383.
B. Kopeliovich et al., *Zeit. Phys.* **C73** (1996) 125.

[33] K. Schilling, G. Wolff, *Nucl. Phys.* **B61** (1973) 381.

[34] H1 Collab., Conf. Paper 564, 29th Intern. Conf. on HEP, Vancouver, Canada (1998).

[35] F. Gilman et al., *Phys. Lett.* **B31** (1970) 387.
T. Bauer et al., *Rev. Mod. Phys.* **50** (1978) 261.

[36] ZEUS Collab., addendum to Conf. Papers 792, 793, 29th Intern. Conf. on HEP, Vancouver, Canada (1998).

[37] D. Ivanov, R. Kirschner, *Phys. Rev.* **D58** (1998) 114026

[38] ZEUS Collab., J.Breitweg et al., DESY **98-107**, submitted to Eur. Phys. J. C

[39] M. Ryskin, *Sov. J. Nucl. Phys.* **52** (1990) 529.
N. Nikolaev, B. Zakharov, *Z. Phys.* **C53** (1992) 331.
M. Wüsthoff, *Phys. Lett.* **D56** (1997) 4311.
W. Buchmüller et al., *Nucl. Phys.* **B487** (1997) 283.
W. Buchmüller et al., DESY **98-113**, *hep-ph/9808454*.

[40] J. Bartels et al., , DESY **98-034**, *hep-ph/9803497*.

[41] M. Glück et al., *Z. Phys.* **C53** (1992) 651.
M. Glück et al., *Z. Phys.* **C67** (1995) 433.

[42] ZEUS Collab., J. Breitweg et al., *Phys. Lett.* **B421** (1998) 368.
H1 Collab., C. Adloff et al., *Eur. Phys. J.* **C1** (1998) 495.

[43] H1 Collab., C. Adloff et al., *Phys. Lett.* **B428** (1998) 206.
ZEUS Collab., Conf. Paper 787, 29th Intern. Conf. on HEP, Vancouver, Canada (1998).

[44] H1 Collab., C. Adloff et al., *Eur. Phys. J.* **C5** (1998) 439.

[45] ZEUS Collab., J. Breitweg et al., DESY **98-045**, submitted to *Eur. Phys. J.*

[46] H1 Collab., C. Adloff et al., DESY **98-092**, Submitted to *Eur. Phys. J.*

[47] ZEUS Collab., Conf. Paper 785, 29th Intern. Conf. on HEP, Vancouver, Canada (1998).
H1 Collab., Conf. Paper 558, 29th Intern. Conf. on HEP, Vancouver, Canada (1998).

[48] ZEUS Collab., M. Derrick et al., *Zeit. Phys.* **C68** (1995) 569.

[49] P. Bruni, G. Ingelman, proc. Int. Europhys. Conf. on HEP, Marseilles, July 1993, 595.

[50] J. Bjorken, *Phys. Rev.* **D47** (1993) 101.
E. Gotsman, E. Levin, U. Maor, *Phys. Lett.* **B309** (1993) 199.
E. Gotsman, E. Levin, U. Maor, *Phys. Lett.* **B438** (1998) 229.

[51] H. Jung, *Comp. Phys. Commun.* **86** (1995) 147.

[52] J. Bartels et al., *Phys. Lett.* **B379** (1996) 239.
J. Bartels et al., *Phys. Lett.* **B386** (1996) 389.